Knot Segmentation in Noisy 3D Images of Wood

A. Krähenbühl, B. Kerautret, and I. Debled-Rennesson

Université de Lorraine, LORIA, Adagio team, UMR 7503, 54506, Nancy, France

Abstract. Resolving a 3D segmentation problem is a common challenge in the domain of digital medical imaging. In this work, we focus on another original application domain: the 3D images of wood stem. At first sight, the nature of wood image looks easier to segment than classical medical image. However, the presence in the wood of a wet area called sapwood remains an actual challenge to perform an efficient segmentation. This paper introduces a first general solution to perform knot segmentation on wood with sapwood. The main idea of this work is to exploit the simple geometric properties of wood through an original combination of discrete connected component extractions, 2D contour detection and dominant point detection. The final segmentation algorithm is very fast and allows to extract several geometrical knot features.

Keywords: 3D segmentation, dominant points, histogram, geometrical features, wood knot.

1 Introduction

Outside the classical medical applications, 3D digital imaging systems like X-Ray Computer Tomography are an interesting way for biologists to analyze wood. Even less frequent, these original images could offer the possibility to access to numerous geometric informations about wood knots [12]. A wood knot is the young part of a branch included in the wood stem (see Fig. 1(b)). Sawmills are also interested by knot segmentation in 3D images to optimize the cutting decisions of wood planks. They expect to improve at the same time the wood plank appearance and the productivity.

By nature, wood structures are simpler to segment than medical images. At first view, the extraction of wood knot does not seem difficult on ideal configurations as in Fig. 1(a). On the contrary, the image 1(b) remains an important problem to apply segmentation. A simple threshold is no more possible since sapwood and knot are connected and of similar intensity. The problem of sapwood is a well known major difficulty.

More precisely, several authors have tried to remove the limitations induced by sapwood. We can cite Andreu and Rinnhofer who propose a specific method based on knot model to segment knots [5]. Their approach is robust on sapwood but is limited to the Norway spruce. Moreover, it can only detect knots with particular orientation specific to the species. This approach can not detect the correct knot structure inside sapwood. Another approach was proposed by Aguilera *et al.* [2]. They use a 2D deformable model with simulated annealing. Their
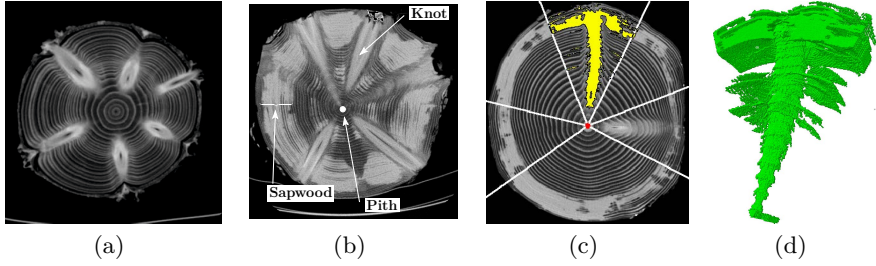
(a)   (b)   (c)   (d)

Fig. 1. Illustration of different knot qualities in X-Ray images. Image 1(a) is an ideal configuration without sapwood, image 1(b) is an noisy version with sapwood. Images 1(c) and 1(d) show the limitations of the previous proposed approach [9].

approach can give results in presence of sapwood but an important separation is visible between knot and sapwood on the examples of their experiments. The proposed method also suffers from the setting of the deformable model parameters. Moreover, it is not automatic: the deformable model must be manually initialized. We can also refer to the work of Nordmark [14]. He proposes to use neural networks to solve the knot detection problem in presence of sapwood. This original solution is interesting but presents the main inconvenients to be very slow and does not always provide precise results. Note that other classical segmentation approaches, like the 3D deformable models, are also not able to perform knot segmentation in presence of sapwood (see for instance the segmentation comparison in [9] or the one of Fig 10(f).

In previous work, we proposed a sapwood robust approach to detect position and orientation of knots [9]. This first step is only limited to the detection and does not segment the knots. In particular, the limits of such approach are illustrated on Fig. 1(c) and 1(d). The contribution of this new paper is to advance further than the previous detection by performing a real segmentation even in presence of sapwood. The main idea of the proposed method is to exploit geometric information analyzed from the discrete contour of 2D images. Through this method, we can integrate an *a priori* shape knowledge on knot and sapwood while remaining efficient.

Before introducing this new solution, we summarize in the following section the previous work of knot area detection which represents an important step in the proposed method. Afterwards, we detail our knot segmentation method. Finally, we present our results and comparisons with results of recent segmentation algorithms.

2   Knot Areas Detection

In previous work, we present an histogram based method to isolate each tree knot in an angular interval [9]. Since our work relies on this detection we recall here the main steps of the algorithm.
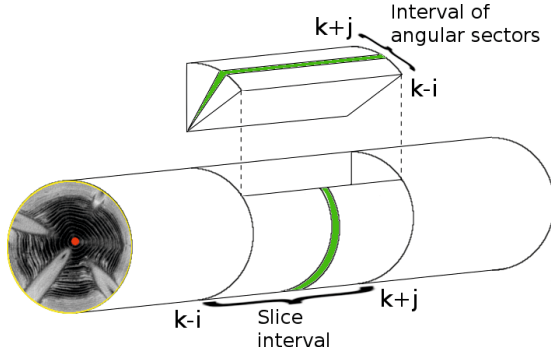
Fig. 2. Schema of the detection of slice intervals and angular intervals. In green a slice and an angular sector corresponding to a peak in the z-motion histograms and pie-charts. The $[k-i, k+j]$ intervals are the computed intervals from each peaks.

We work with a 3D grey level image I of $N \times M \times K$ resolution. A slice S_k of size $N \times M$ is a subimage of I corresponding to a cross-section of the tree. S_1 and S_K correspond respectively to the bottom and the top of tree when it is scanned from bottom to top. We work also with the pith. Biologically, the pith is the tree center, the growth rings center and the most important for us, the knot origin. To localize the pith, we use an algorithm proposed by Fleur Longuetaud [11] based on the growth rings detection. The pith position is defined as the intersection point of the lines perpendicular to the growth rings. We obtain one pixel by slice. The pith position will be used like center of all the angular sectors.

The z-Motion. By sliding the slices, we can observe that knots move from the pith to the bark. Only the knots produce big motions due to a big contrast with softwood. We name this motion the z-motion.

Definition 1. *Let $(S_k)_{k \in [1,K]}$ be a set of K slices. The z-motion slice Z_k is defined as the absolute value of intensity variation between the two consecutive slices S_{k-1} and S_k :*

$$Z_k = |S_k - S_{k-1}|$$

The set of Z_k images provides a new 3D image of dimension $N \times M \times K - 1$ where a big value implies a big motion. It is not a problem to have the first slice S_1 without corresponding z-motion slice. It is the first or the last slice and we ignore these slices during the stem analysis: they are too noisy. The set of Z_k is used to identify slice intervals containing knots. In each of them, we identify the angular intervals containing knots.

Let us see now how to use z-motion to determine slice intervals and angular intervals containing knots.

2.1   Slice and Angular Intervals

The first detection identifies the slice intervals (see Fig. 2). To determine these intervals, we construct the histogram of z-motion sum (see Fig. 3). Each value represents the sum of all pixels of a slice Z_k. The peaks correspond to a slice with a lot of big motions, meaning that we are in presence of knots. The algorithm to determine significant peaks and the corresponding intervals is based on the analysis of derivative gradient. It is detailed in [9].
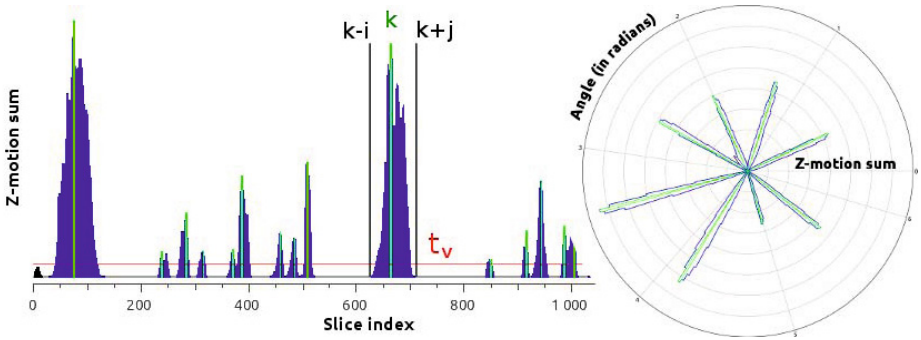

Fig. 3. Histogram and pie-chart of z-motion sum. In each of them, we identify knot intervals with the same algorithm.

Usually, the knots constitute a whorl[1]. This implies that there are several knots in a slice interval. To isolate each knot of a whorl, we proceed to a second analysis of z-motion in each slice interval $[Z_{k-i}, Z_{k+j}]$. Each slice is divided in 360 angular sectors centered on the pith. We construct the pie-chart of z-motion sum illustrated on the Fig. 3. One value corresponds to the z-motion sum on a same angular sector taken on all the slices of $[Z_{k-i}, Z_{k+j}]$. In the same way than for the slices, we compute intervals of angular sectors. An angular interval is a set of consecutive angular sectors containing just one knot (see Fig. 2).

3   A Suitable Segmentation in Angular Intervals

Let I be a billon's image of size $N \times M \times K$. I can be seen as a sequence of slices $(\mathcal{S}_k)_{k \in [1,K]}$ or as a sequence of angular sectors $(s_d)_{d \in [1,D]}$. After the detection process of slice intervals (see Section 2), we obtain a set (i_x) of slice intervals. The original image I restricted to an interval i_x generates a slice subsequence $\mathcal{P}_x$ (see Fig. 4).

A detection process of angular sector is applied to each slice subsequence $\mathcal{P}_x$. This process furnishes a set (α_y) of angular intervals with usually just one

---

[1] Knot group with the same origin, the pith, and organized in circle around the pith axis (see Fig. 1(a)).
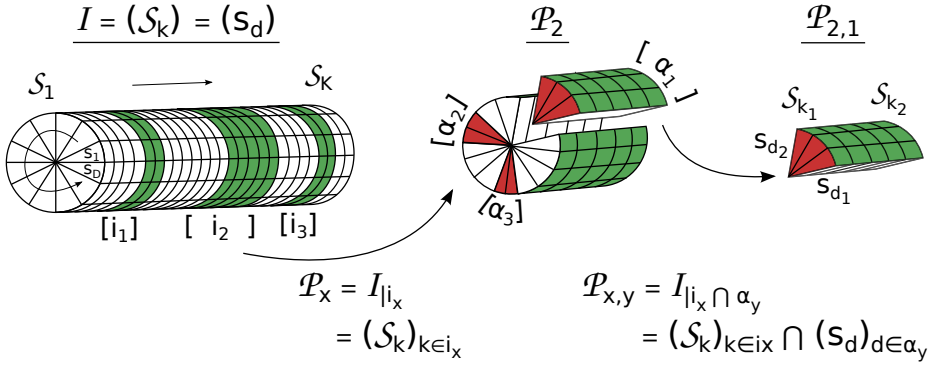
Fig. 4. Notation illustration

knot. The slice interval $\mathcal{P}_x$ restricted to an angular interval α_y is an angular subsequence $\mathcal{P}_{x,y}$ similar to a piece of pie. In the following, we name " knot area " the subsequences $\mathcal{P}_{x,y}$ (see on the right of the Fig. 4).

The segmentation process described in this section is applied to each knot area $\mathcal{P}_{x,y}$. It begins by a 3D connected component extraction based on the grey level. The objective of this extraction is to eliminate the connected components resulting from noise as growth rings. The chosen threshold is -100 to be sure to not cut the knots (in general fixed beetween -90 and -70 by biologists). As a reminder, the grey level interval corresponding to the wood density in X-Ray images is $[-900, 530]$. As a result, we obtain one or more connected components and we keep the biggest (within the meaning of voxel number) in a new binary knot area $\mathcal{B}_{x,y}$ with the same dimensions than $\mathcal{P}_{x,y}$.

The proposed algorithm is applied on each 2D slice $S_{x,y}$ of $\mathcal{B}_{x,y}$. It consists of the four main steps described in the following sub-sections (see Fig. 5).

3.1   Step 1: 2D Connected Component Extraction

The first step consists in a 2D connected component extraction applied on $S_{x,y}$. It potentially contains a part of the biggest connected component of $\mathcal{B}_{x,y}$. We can have more than one connected component in the 2D slice $S_{x,y}$ while $\mathcal{B}_{x,y}$ contains only one connected component. It is a previous or a next slice of $\mathcal{B}_{x,y}$ that merges the different connected components of $S_{x,y}$.

After the 2D connected component extraction, we keep the components with more than 15^2 pixels. We name this new slice $S'_{x,y}$. In Fig. 5(a), we have an example of $S'_{x,y}$ with just one connected component drawn in pink. The two dark pink lines represents the bounds of the α_y angular interval.

3.2   Step 2: Contour Detection

We search P_0 in $S'_{x,y}$, the nearest pixel to the pith belonging to a 2D connected component found at the previous step. To do this, we use Andres's circle [4]

with an increasing radius. The Andres's circle ensures to visit all the surface of $S'_{x,y}$ by a complete paving of plan. The found pixel P_0, drawn in red and green in Fig. 5(b), is the first point of the contour $\mathcal{C}$. From P_0, we applied an algorithm based on the Moore's neighborhood to determine the other $\mathcal{C}$ points of the nearest connected component of the pith.

To obtain better results in the next step, we smooth the contour $\mathcal{C}$ with an averaging mask of radius 3. It is the smoothed contour $\mathcal{C}^s$ that appears in blue in Fig. 5(b).
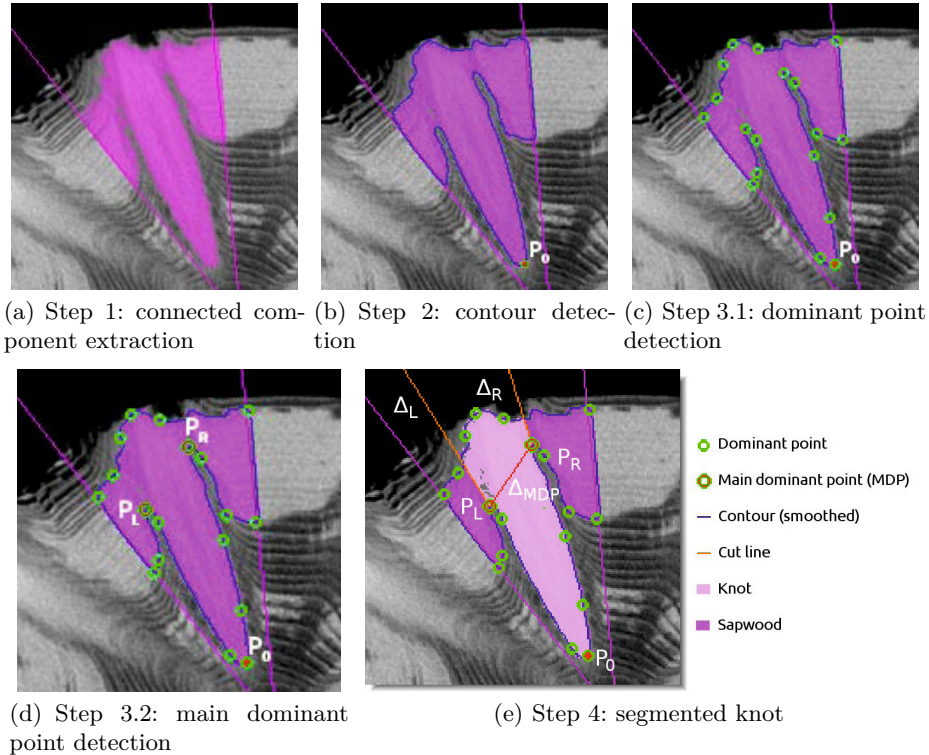

(a) Step 1: connected component extraction (b) Step 2: contour detection (c) Step 3.1: dominant point detection

(d) Step 3.2: main dominant point detection (e) Step 4: segmented knot

Fig. 5. Knot segmentation algorithm in four steps

3.3   Step 3: Dominant Points

The objective of this step is to find the junction points P_L and P_R between knot and sapwood inside the smoothed contour $\mathcal{C}^s$. The proposed method uses the dominant point notion (characteristic points of the contour) and a criterion based on distances to the pith to discriminate them.

Step 3.1: Dominant Point Detection. We detect the dominant points of $\mathcal{C}^s$ with a method proposed by Nguyen et al. in [13]. The algorithm relies on arithmetical discrete lines [16] and blurred segments [7].

The notion of blurred segment was intro-
duced from the notion of arithmetical dis-
crete line. An arithmetical discrete line, noted
$D(a, b, \mu, \omega)$, is a set of points $(x, y) \in \mathbb{Z}^2$ that
verifies $\mu \leq ax - by < \mu + \omega$. A blurred seg-
ment with a main vector (b, a), lower bound μ
and thickness ω is a set of integer points (x, y)
that is optimally bounded (see [7]) for more
details) by a discrete line $D(a, b, \mu, \omega)$. The
value $\nu = \frac{\omega - 1}{max(|a|,|b|)}$ is called the width of
this blurred segment. The upper figure shows

Fig. 6. A blurred segment

a blurred segment (the sequence of gray points) whose the optimal bounding
line is $D(5, 8, -8, 11)$.
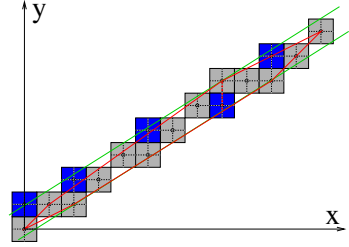
Nguyen et al. proposed the notion of maximal blurred segment. A maximal
blurred segment of width ν (see Fig. 6) is a blurred segment that can not be
extended to the left and the right sides. A linear recognition algorithm of width
ν blurred segments [7] permits for a given contour $\mathcal{C}$ to obtain the sequence
$\mathcal{S}_{\mathcal{C}_\nu}$ of all its maximal blurred segments of width ν. We then scan the sequence
$\mathcal{S}_{\mathcal{C}_\nu}$: in each smallest zone of successive maximal blurred segments whose slopes
are increasing or decreasing, the candidate as dominant point is detected as the
middle point of this zone.

This method is used on the $\mathcal{C}^s$ contour detected at the previous step on the
$S'_{x,y}$ slice, with a width $\nu = 3$. Let $(P_n)_{1 \leq n \leq N_P}$ be the sequence of the N_P
dominant points obtained on the $\mathcal{C}^s$ contour (see example in Fig. 5(c)).

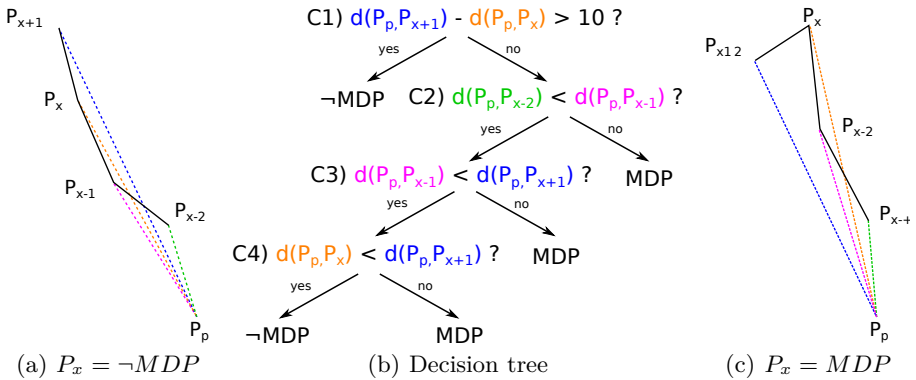(a) $P_x = \neg MDP$ (b) Decision tree   (c) $P_x = MDP$

Fig. 7. Decision tree of the MDP criterion with illustration of two different executions.
In (a), C1 is false and C2, C3 and C4 are true. In (c), C4 is false.

Step 3.2: Main Dominant Points Detection. We want to identify the two main dominant points (MDP), P_L and P_R, with $L, R \in [1, N_P]$, $L < R$ and respectively on the left and on the right of P_0 (see Fig. 5(d)). The left and right sides are defined from the pith position and the orientation of the α_y angular interval: left in counterclockwise, right in clockwise. We are still working on the slice $S'_{x,y}$ and the two points make the junction between knot and sapwood on this slice.

We test successively each dominant point P_n with the decision tree presented in Fig. 7. They are tested in clockwise from P_1 to determine P_L and in counterclockwise from P_{N_P} to determine P_R.

For each dominant point P_x, the MDP criterion is based on the euclidean distances d between the pith point P_p and four dominant points:

- P_{x-2}, P_{x-1}, P_x and P_{x+1} when we search P_L,
- P_{x+2}, P_{x+1}, P_x and P_{x-1} when we search P_R.

The Fig. 7 presents the tree decision and examples of the MDP criterion for P_L. The first condition C_1 ensures that P_x is not a MDP when the next dominant point P_{x+1} moves far enough away from the pith (more than 10 pixels) relatively to P_x. The following conditions C_2 to C_4 ensure a distance order such as $d(P_p, P_{x-2}) < d(P_p, P_{x-1}) < d(P_p, P_{x+1})$. These conditions reflect the stem shape and the pith circularity: they identify the first dominant point that does not move away from the pith.

The main dominant point detection furnishes zero, one or two points from which we can separate the knot from the pith. We need to treat the three cases to obtain a segmentation of any slice $S'_{x,y}$.

3.4   Step 4: Knot Segmentation in Sapwood from MDP

From each found MDP, we define a cut line to separate knot from sapwood. These lines are named Δ_L for P_L and Δ_R for P_R. Each of them is built from two points: the considered MDP and the mean point of the previous dominant points for P_L, respectively the following dominant points for P_R. Moreover, we define the segment Δ_{MDP} linking P_L to P_R when we find two MDP (see Fig. 8(c)).

We consider three cases depending on the number of MDP, illustrated by the Fig. 8. On each of them, the light pink area corresponds to the segmented knot.

No MDP. In this case we considered that all the connected component of $S'_{x,y}$ corresponds to the knot. There are two typical cases involving no MDP detection:

- when the knot and the sapwood are not connected (see Fig. 8(a)),
- when the knot is completly included in the sapwood.

One MDP. When there is only one MDP, P_L or P_R, the part of the connected component section corresponding to the knot is:

- on the right to P_L if P_L is the detected MDP (see Fig. 8(b)),
- on the left to P_R if P_R is the detected MDP.

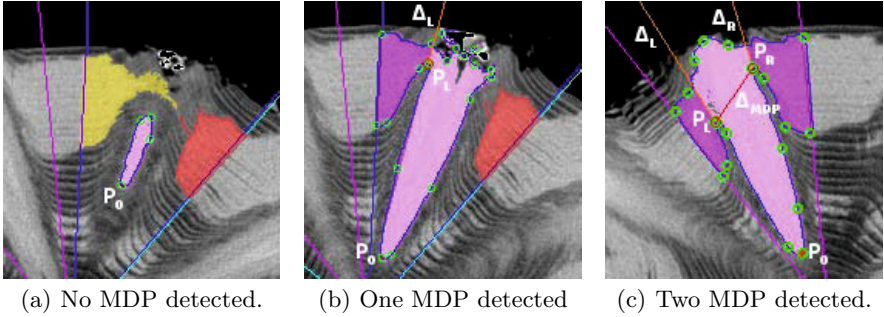(a) No MDP detected.   (b) One MDP detected   (c) Two MDP detected.

Fig. 8. Knot estimation based on the number of main dominant points

Two MDP. It is the most common case. It occurs most often when the knot is in contact whith the sapwood. In this case, we define the segment Δ_{MDP} which allows to separate the knot in two parts: the upper part and the lower part. They correspond respectively to the knot parts inside and outside the sapwood (see Fig. 8(c)).

We segment separately the two parts. The lower part is segmented by defining a contour $\mathcal{C}_1$. $\mathcal{C}_1$ is composed of the two parts of $\mathcal{C}^s$, (P_R, P_0) and (P_0, P_L), and the segment Δ_{MDP}. All pixels inside $\mathcal{C}_1$ and belonging to the considered connected component of $S'_{x,y}$ belong to the knot. The second part, above the Δ_{MDP} so inside the sapwood, is a restricted area of the considered connected component of $S'_{x,y}$. It is the connected component part simultaneously on the right of Δ_L, on the left of Δ_R and on the top of Δ_{MDP}.

The fusion of the two parts produces the segmented knot of the slice $S'_{x,y}$, in light pink in Fig. 8(c).

The four steps of algorithm allow to segment a knot on a 2D slice $S_{x,y}$ of a 3D knot area $\mathcal{P}_{x,y}$. By merging all 2D segmented knots, we obtain the 3D reconstruction of the knot of $\mathcal{P}_{x,y}$. But all slices of $\mathcal{P}_{x,y}$ do not contain part of the knot. It is necessary to detect in $\mathcal{P}_{x,y}$ the interval $[l, u]$ of slices containing a part of the knot to obtain a clean 3D reconstruction. In fact, the slices outside $[l, u]$ contain just sapwood that the algorithm can segment as on the right of Fig. 9. It is usually the case but we can see that the segmented connected component does not contain knot. The $[l, u]$ detection allows to reconstruct knot with just slices containing a part of knot.

The slice interval $[l, u]$ is computed from the distance to the pith of the first dominant point P_0 in each slice $S_{x,y}$ of a knot area $\mathcal{P}_{x,y}$. We construct the corresponding histogram H, illustrated on Fig. 9. In this histogram, we can detect the knot interval $[l, u]$. The process starts with the localization of the minimum, in red on Fig. 9. Afterwards, we seek the bounds l and u (in green on Fig. 9) on each side of the minimum. A slice index j is the lower bound l, respectively the upper bound u, if $H_{j-6} - H_{j-1} < 5$, respectively if $H_{j+6} - H_{j+1} < 5$.
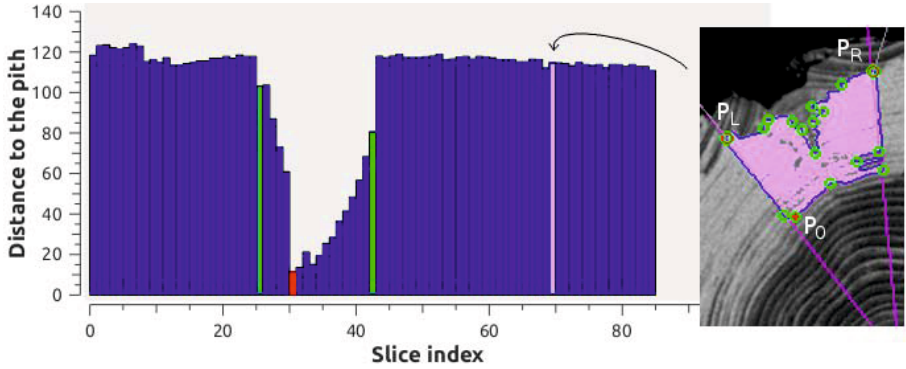
Fig. 9. Histogram of distances to the pith of a knot area $\mathcal{P}_{x,y}$. On the right, an example af sapwood segmentation in a slice without knot.

(a)   (b)   (c)* Interactive 3D view
                                                                              with acrobat reader.

(d)   (e)   (f)* Interactive 3D view
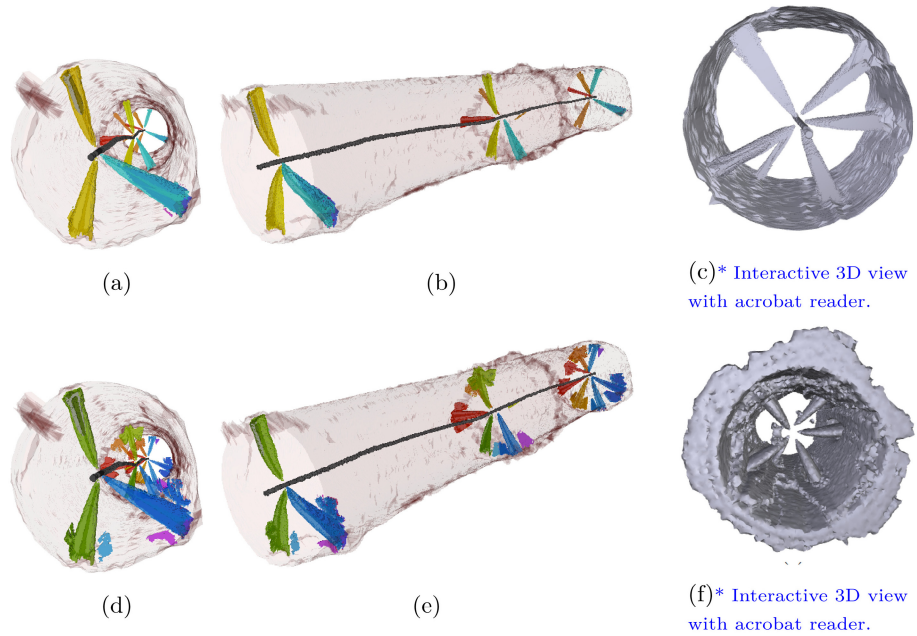   with acrobat reader.

Fig. 10. Illustration of the segmentation results of the proposed approach (images (a,b)) and comparisons with previous work (images (d,e)) [9]. Images (c,f) show comparison between our approach (c) and deformable model (f) [10]. The static and dynamic visualizations were generated with the *DGtal* library [1].
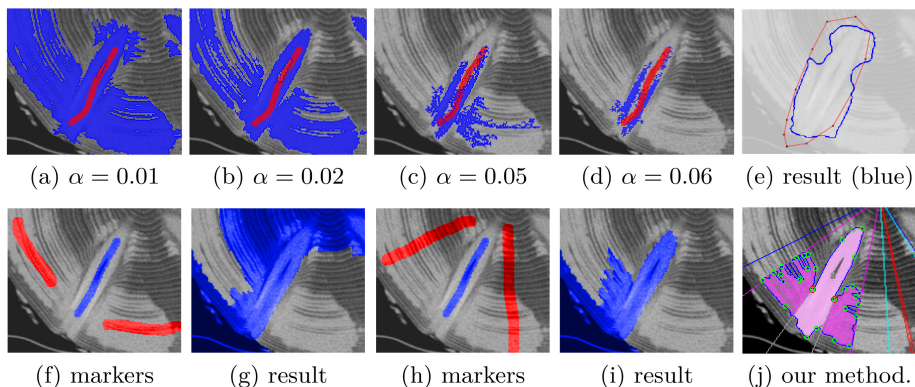
(a) $\alpha = 0.01$ (b) $\alpha = 0.02$ (c) $\alpha = 0.05$ (d) $\alpha = 0.06$ (e) result (blue)

(f) markers   (g) result   (h) markers   (i) result   (j) our method.

Fig. 11. Experiments of various segmentation methods on the bottom left part of image of Fig. 1(b). Images (a-d) show results obtained from a Component Tree based approach [15] with different values of the user parameter α. Result of morphological snake [3] is given in (e) and *power watersheds* [6] algorithm result is displayed with two configurations of markers (images (f-i)). The result of our algorithm is displayed in image (j) in light pink color.

4   Experiments and Comparisons

To evaluate the efficiency of our approach, the knot segmentation was applied on a difficult sample of spruce containing continue areas of sapwood. The segmentation results are presented on images (a-c) of Fig. 10. Note that we focus on the extraction of the larger branches by constraining the segmentation from a threshold on the minimal size of the segmented component. As comparison, the basic knot segmentation (images (d,e)) is performed with a simple threshold on the knot areas detected from previous work [9]. As shown in figure Fig. 10, our approach is able to remove all sapwood areas without any markers.

Comparisons with Other Approaches. Before defining the proposed approach, we experimented several recent and promising segmentation methods. The first one is the method of the Component Tree [15]. Even with a manual adjustment of the markers and the numeric parameter, we can see that result does not fit to the initial knot (images (a-d)) of Fig. 11. We also apply the *power watersheds* [6] and morphological snake algorithms [3] respectively on images (e) and (f-i). As comparison, the result of our segmentation method is displayed in image (j). The images (c,f) of Fig. 10 complete the comparisons of our algorithms (image (c)) with a 3D deformable model [10]. Contrary to our approach, the 3D deformable model also segments together the sapwood with the knots.

5   Conclusion

This paper proposes a segmentation method applied to the wood knot problem. Known as a difficult problem, we use histograms and discrete tools to propose a

new solution. The resulting approach is efficient (running time around few minutes for a complete log, without optimization) in comparison to 3D deformable model [10] (order of hours for the sample of Fig. 10). Some improvements can be done in future work to apply segmentation on large and small knots simultaneously. The source code of the algorithm is available online [8].

References

1. DGtal: Digital geometry tools & algorithms library, `http://libdgtal.org`
2. Aguilera, C., Sanchez, R., Baradit, E.: Detection of knots using x-ray tomographies and deformable contours with simulated annealing. Wood Res. 53, 57–66 (2008)
3. Alvarez, L., Baumela, L., Márquez-Neila, P., Henríquez, P.: A real time morphological snakes algorithm. Image Processing On Line (2012)
4. Andres, E.: Discrete circles, rings and spheres. Comp. & G. 18(5), 695–706 (1994)
5. Andreu, J.P., Rinnhofer, A.: Modeling Knot Geometry in Norway Spruce from Industrial CT Images. In: Bigun, J., Gustavsson, T. (eds.) SCIA 2003. LNCS, vol. 2749, pp. 786–791. Springer, Heidelberg (2003)
6. Couprie, C., Grady, L., Najman, L., Talbot, H.: Power watersheds: A unifying graph-based optimization framework. IEEE PAMI 33(7), 1384–1399 (2010)
7. Debled-Rennesson, I., Feschet, F., Rouyer-Degli, J.: Optimal blurred segments decomposition of noisy shapes in linear time. Comp. & Graphics 30(1), 30–36 (2006)
8. Krähenbühl, A.: (2012), `https://github.com/adrien057/TKDetection/tags/`
9. Krähenbühl, A., Kerautret, B., Debled-Rennesson, I., Longuetaud, F., Mothe, F.: Knot Detection in X-Ray CT Images of Wood. In: Bebis, G., Boyle, R., Parvin, B., Koracin, D., Fowlkes, C., Wang, S., Choi, M.-H., Mantler, S., Schulze, J., Acevedo, D., Mueller, K., Papka, M. (eds.) ISVC 2012, Part II. LNCS, vol. 7432, pp. 209–218. Springer, Heidelberg (2012)
10. Lachaud, J.O., Taton, B.: Deformable model with adaptive mesh and automated topology changes. In: Proc. 3DIM (2003)
11. Longuetaud, F., Leban, J.M., Mothe, F., Kerrien, E., Berger, M.O.: Automatic detection of pith on ct images of spruce logs. Computers and Electronics in Agriculture 44(2), 107–119 (2004)
12. Longuetaud, F., Mothe, F., Kerautret, B., Krähenbühl, A., Hory, L., Leban, J.M., Debled-Rennesson, I.: Automatic knot detection and measurements from x-ray ct images of wood: A review and validation of an improved algorithm on softwood samples. Computers and Electronics in Agriculture 85, 77–89 (2012)
13. Nguyen, T.P., Debled-Rennesson, I.: A discrete geometry approach for dominant point detection. Pattern Recognition 44(1), 32–44 (2011)
14. Nordmark, U.: Value Recovery and Production Control in the Forestry-wood Chain Using Simulation Technique. Ph.D. thesis, Luleå University of Technology (2005)
15. Passat, N., Naegel, B., Rousseau, F., Koob, M., Dietemann, J.L.: Interactive segmentation based on component-trees. Pat. Rec. 44(10-11), 2539–2554 (2011)
16. Reveillès, J.P.: Géométrie discrète, calculs en nombre entiers et algorithmique (Discrete geometry, integers calculus and algorithmics). Ph.D. thesis, Université Louis Pasteur, Strasbourg (1991), thèse d'état